JOURNAL OF MATERIALS SCIENCE 8 (1973) 1439–1448

Investigation of short range ordering in polymers by means of radial distribution functions derived from X-ray diffraction

Part 1 *Bisphenol-A polycarbonate*

G. D. WIGNALL, G. W. LONGMAN
Imperial Chemical Industries Limited, Corporate Laboratory, Runcorn, Cheshire, UK

Two samples of bisphenol-A polycarbonate, showing marked differences in impact behaviour due to different thermal histories, were investigated by radial distribution function (RDF) methods. The RDF patterns were virtually identical and showed that the short range order (0 to 10 Å) in the samples had been essentially unaffected by the annealing procedures. Most of the intra-molecular distances in the polymer repeat unit were successfully resolved in the RDF pattern. However, there were only suggestions of broad peaks at $r \sim 5.5$ Å and $r \sim 10$ Å attributable to intermolecular ordering, indicating that little intermolecular ordering had occurred in either sample. Explanations of the different impact properties of the two samples which assume a significant short range re-ordering on annealing are thus ruled out on the available evidence.

A more highly annealed sample was examined to assess the sensitivity of the RDF method to short range intermolecular ordering. The RDF plot of this sample showed a marked periodicity peaking at intervals of ~ 5.5 Å which was attributed to intermolecular ordering, thus confirming the above conclusion.

1. Introduction

Studies of the impact properties of bisphenol-A polycarbonate have revealed a marked dependence of the impact strength on the thermal history of the sample [1]. In particular when "amorphous" polycarbonate is annealed at 120° C for 3 h, the room temperature impact strength falls by more than a factor of seven. ("Amorphous" samples were prepared by injection moulding with a mould temperature of 90° C, and removing samples from the mould as soon as possible.) The structure of the material is "amorphous" both before and after annealing, when judged by the widely used criterion that the material does not give an X-ray diffraction pattern comprising sharp Bragg reflections. It has been suggested [1] that short-range re-ordering or "crystallization" might take place on annealing, which would not give rise to sharp Bragg reflections if the ordered regions remained very small. The short range order in "amorphous" materials can be characterized precisely by means of radial distribution function (RDF) methods [2], derived from a careful analysis of the scattered diffraction pattern from the material. These techniques have been used to examine the two samples described above, and a more ordered specimen annealed at 190° C for 122 h. The latter sample was included to show that RDF techniques can reveal short range ordering in partially ordered high polymers when the level of ordering remains comparatively low.

2. Theory

The structure of non-crystalline solids is specified in terms of radial distribution functions. If there are several different types of atom in the system A, B, C, D etc, then we may define a series of partial RDFs, $g_{ij}(r)$, by

$$g_{ij}(r) = \frac{\rho_{ij}(r)}{\bar{\rho}_j} \qquad (1)$$

where $\rho_{ij}(r)$ is the density (number per unit volume) of j-type atoms at a distance r from an

i-type atom, and ρ_j is the average density of j-type atoms in the whole system (i.e. the total number of j-type atoms divided by the total volume). Thus for example $g_{AB}(r)$ is a measure of the way in which B-type atoms are correlated in distance around A-type atoms. It is convenient to define $h_{ij}(r)$ by

$$h_{ij}(r) = g_{ij}(r) - 1 \ . \tag{2}$$

In principle it is possible to determine each $h_{ij}(r)$ for the system by means of radiation scattering experiments. The rigorous theory of scattering from a system containing more than one kind of atom has been given by Waser and Schomaker [2], and discussed by Pings and Waser [3] whose notation is adopted in this paper. The intensity of radiation, $I_{coh}(2\theta)$, scattered coherently from a sample is measured as a function of the scatter angle 2θ, over as wide a range as possible in the experiment. The scattering variable is conventionally converted from 2θ to $s = 4\pi/\lambda \sin \theta$ where λ is the wavelength of the incident and (elastically) scattered radiation and $I_{coh}(s)$ is corrected for experimental conditions (see Section 4). Pings and Waser defined $i(s)$ by

$$i(s) = \left[\frac{I_{coh}(s)}{N} - \sum_{i=1}^{n} x_i f_i^2(s)\right] \Bigg/ \left[\sum_{i=1}^{n} x_i f_i(s)\right]^2 \tag{3}$$

where N is the total number of atoms; n is the number of species in the system; $f_i(s)$ is the scattering factor of the ith species; x_i is the atomic fraction of species i, and $I_{coh}(s)$ has been normalized to electron units (see Section 4).

If we define $F_{ij}(s)$ by

$$F_{ij}(s) = f_i(s)f_j(s)/[\sum_{i=1}^{n} x_i f_i(s)]^2 \tag{4}$$

where the Fourier transform of $F_{ij}(s)$ is given by

$$J_{ij}(r) = \pi^{-1} \int_0^\infty F_{ij}(s) \cos rs \, ds \tag{5}$$

and $H(r)$ by

$$\bar{\rho} r H(r) = \frac{1}{2\pi^2} \int_0^\infty si(s) \sin rs \, ds \tag{6}$$

where $\bar{\rho}$ is the average (number) density of atoms in the system, i.e. the total number of atoms, N, divided by V, the volume of the system, it may be shown that

$$H(r) = \sum_{i=1}^{n} \sum_{j=1}^{n} x_i x_j H_{ij}(r) \tag{7}$$

where

$$H_{ij}(r) = r^{-1} \int_{-\infty}^{+\infty} y h_{ij}(y) \, J_{ij}(r-y) \, dy. \tag{8}$$

To understand the physical significance of these equations, consider the case of neutron scattering where f is a constant independent of s. Thus F_{ij} is a constant independent of s and thus $J_{ij}(r)$ becomes a delta function apart from a proportionality factor, and Equation 7 then becomes

$$H(r) = \sum_{i=1}^{n} \sum_{j=1}^{n} x_i x_j \frac{f_i f_j}{\left[\sum_{i=1}^{n} x_i f_i\right]^2} h_{ij}(r) \ . \tag{9}$$

Thus by measuring the scattered intensity over as wide a range as possible, normalizing to electron units (Equation 3), its Fourier transform (Equation 6) gives a weighted average of the different atomic correlation functions (Equation 9). The correlation functions are weighted by the atomic concentrations of the atoms and their scattering factors.

For X-ray measurements the f_i have different weightings for different atoms and thus different atomic correlations are highlighted. A complication arises in that the f_i are now s dependent for X-rays and although all f_i have approximately the same functional form, the ratio F_{ij} of the f_i (Equation 4) turns out to be s dependent. Thus there is no clear separation of $J_{ij}(r)$ into a delta function and $H(r)$ into a weighted average of the different atomic correlation functions.

In principle this problem could be overcome by restricting measurement to systems where different nuclear isotopes are available. These isotopes in general have different neutron scattering cross-sections f_i and thus in a binary system (say) one could perform three different scattering experiments with different isotopes and hence extract the three different atomic correlation functions $h_{ij}(r)$ [3, 4]. Although this is the most satisfactory approach it is restricted to systems where the different isotopes exist and are available, thus ruling out most systems of interest. Even in systems where this approach

is feasible, no experiment has yet succeeded in obtaining the correlation functions.

An alternative approach to this problem which has been extensively used in X-ray investigations of the structure of non-crystalline solids [5] is to take advantage of the fact that $F_{ij}(s)$ is only *weakly* dependent upon s. $H(r)$ is formed from the measured $i(s)$ as described above, and the resulting $H(r)$ will then be a weighted sum of the correlation functions convoluted with the J_{ij}. Because the F_{ij} are only weakly dependent on s the effect of the convolution will be a small broadening of the sum of $h_{ij}(r)$ to a good approximation. $H(r)$ will differ only slightly from Equation 9 and the area under each $h_{ij}(r)$ will be unaffected. At this state the most fruitful approach is to compare the structural information obtained with models based upon the crystal structure. This procedure is adopted in this paper. Previous studies [6] of the structure of polycarbonate treated the first amorphous halo as a Bragg peak and attempted to correlate changes in the "Bragg spacing" with applied stress. No attempt was made to derive radial distribution functions.

3. Data collection

Diffraction data are collected on a Picker automatic four circle diffractometer, employing a molybdenum target ($K\alpha$ wavelength, λ = 0.7107 Å) with balanced Zr-Yt Ross filters on the incident beam to monochromatize the incident radiation. The thickness of the filters were chosen to achieve the best accuracy of monochromatic intensity measurements. [7]. The final filter balance was achieved by temporarily transferring them to the diffracted beam and balancing the transmission of the two films on the β reflection (λ = 0.6322 Å) from a single crystal of beryllium acetate. The X-rays were detected by means of thallium activated sodium iodide crystal with pulse height analysis of the detected photons. The windows in the counting electronics were set to accept 95% of the Kα transmission, thus eliminating most of the low and high energy noise pulses. Background noise pulses were detected at a rate of < 1/10 count sec^{-1}.

Two samples of bisphenol-A polycarbonate were examined initially. Sample A comprised an injection moulded sheet (mould temperature ~ 90°C) removed from the mould as soon possible (ρ = 1.1990 g cm^{-3}).

Sample B was a similar sheet that was subsequently annealed at 120°C for 3 h. The latter sample showed a slight increase in density (ρ = 1.2010 g cm^{-3}) and marked changes in impact properties. RDF techniques were used to see if the observed change in impact properties could be correlated with any increase in the short range order within the annealed sample.

The samples, which consisted of plates with rectangular facial dimensions of ~ 2.5 cm × 2.5 cm and thickness of 0.131 cm and 0.117 cm, were aligned in the transmission geometry and positioned by the Picker Automatic Diffractometer to bisect the angle between the incident and diffracted beams (Fig. 1).

In principle, it is desirable to measure the intensity of radiation scattered into a point detector at a scatter angle of 2θ when radiation from a point target is incident on a point sample. Every photon is then scattered through an angle of 2θ. In practice, to achieve a measurable intensity the detectors, sample and target are of finite size so that the measured curve of $I(\theta)$ versus 2θ represents an average over a finite range of scatter angles. When the range of scatter angles is very much less than the curvature of the intensity function, $I(\theta)$ the true scattering curve is measured, though as the range of scatter angles accepted increases the measured curve becomes increasingly distorted. The range of scatter angles accepted is a function of the collimation, the geometry being shown in Fig. 1. The effective target is a rectangle of dimensions 1 mm × 0.75 mm. For most of the data collection the divergence angles α and β are set at 0.5°, and thus, when the detector is positioned at an angle 2θ, rays are detected which have been scattered between $2\theta \pm \frac{1}{2}°$.

The error limits of $\mp \frac{1}{2}°$ represent the extremes of the beam penumbra and therefore the maximum departure from perfect collimation, and most photons are scattered at angles well within these limits. These divergence limits were chosen by measuring the diffraction pattern of a typical amorphous glass and closing the divergence angles down until no detectable difference in the shape of the scattering curve was observed. In order to measure accurately at low angles near the main beam, the divergence angles were halved by use of smaller collimators, and the low angle scan subsequently normalized to the main scan in the angular range θ = 8° to 15°.

Intensities were measured over the range θ = 0.5° to 66.0° at angular intervals of θ = 0.25°, giving a range of $S = 4\pi \sin\theta/\lambda$ of 0.15 to

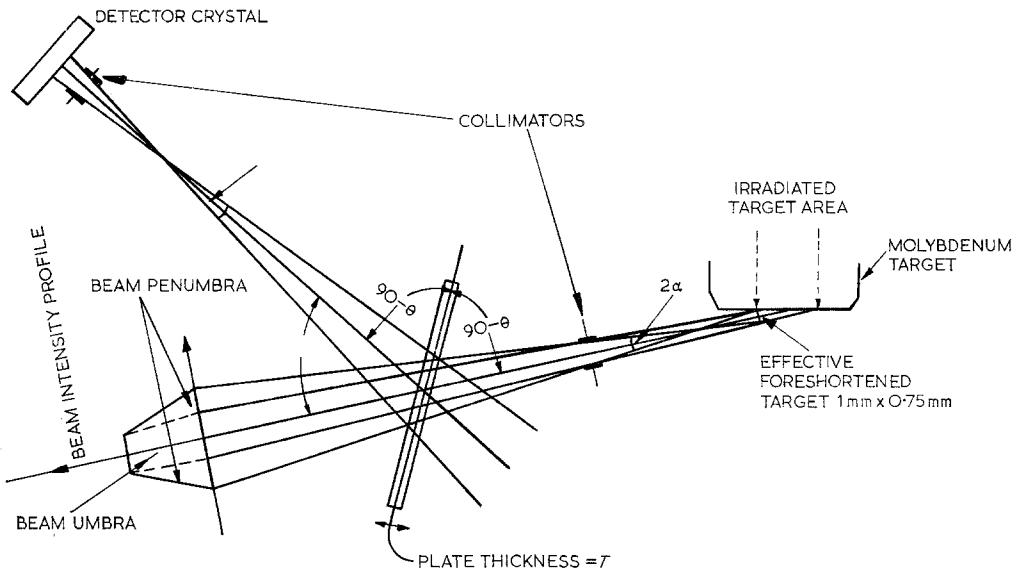

Figure 1 The diffraction geometry.

16.15Å^{-1} where λ is the wavelength of the incident radiation. (λ = 0.7107Å). Data were collected on a fixed count basis, i.e. the time for a fixed count (10000) on each of the two filters (β and α) recorded and converted into a plot of count rate (for a fixed time) by means of a computer programme. Fig. 2 shows a typical plot of $I(\theta) = I^{\beta} - I^{\alpha}$ and a smoothed curve, I_{sm} versus θ corrected for incident intensity drift by repeated checks on the intensity at a fixed angle, every few hours throughout the run. During this period intensity drifts are small (< 2%). Subsequently a third plate (sample C) of similar facial dimensions and thickness 0.096 cm was annealed at 190°C for 122 h. The density of the annealed sample was 1.224 g cm^{-3} indicating that some re-ordering has occurred. The diffraction pattern indicated that the sample was still "amorphous" by the usual criteria, though the peaks were sharper than for samples A and B and therefore smaller scanning intervals ($\triangle 2\theta$ = 0.15°) were used in measuring these peaks.

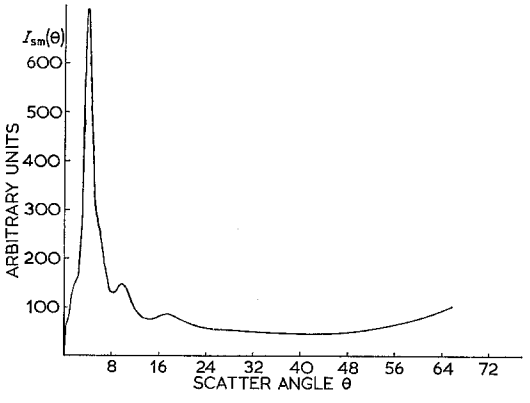

Figure 2 $I_{sm}(\theta)$ versus θ for sample A.

4. Data analysis

The shape of the experimentally measured intensity curve is modulated by the absorption of the incident and diffracted beams in the sample. The modulation will differ for coherent and incoherent scattering owing to the wavelength dependence of absorption and the angle dependent shift in wavelength between the coherent and incoherent wavelengths, λ_c and λ_i respectively.

$$\lambda_i = \lambda_c + 0.024\,(1 - \cos 2\theta)\ . \qquad (10)$$

If a_c denotes the ratio of the coherent scattering per unit volume under hypothetical conditions of no absorption to the coherent scattering actually measured in the geometry of Fig. 1, it may be shown that

$$a_c = \frac{\cos\theta}{AT} \exp(\mu_c T \sec\theta) \qquad (11)$$

where A is the cross-sectional area of the incident beam, T is the plate thickness and μ_c is the linear absorption coefficient for coherent radiation.

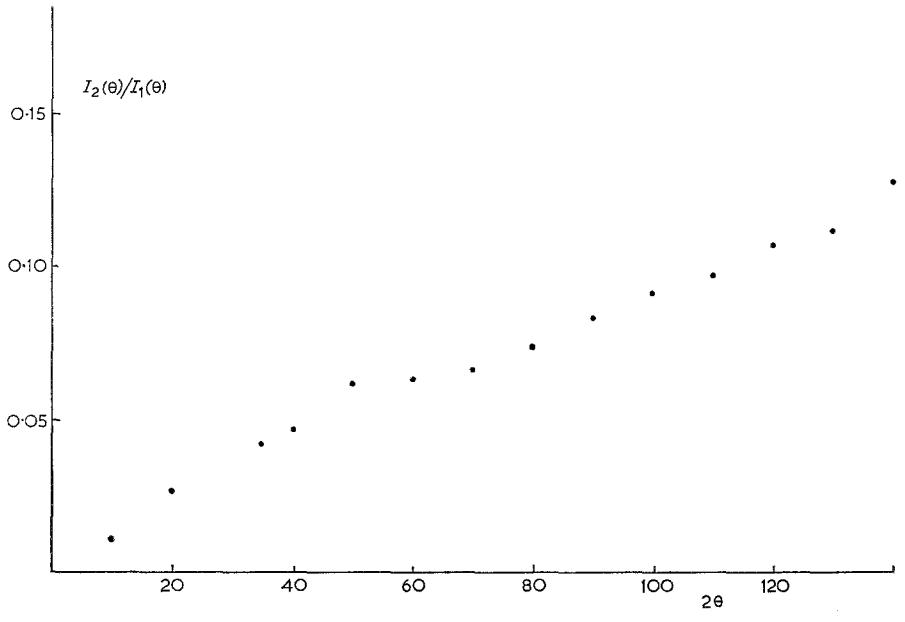

Figure 3 $I_2(\theta)/I_1(\theta)$ versus 2θ for sample A.

Similarly for the incoherent scattering we have, *mutatis mutandis*

$$a_i = \frac{\cos\theta}{AT}\overline{\exp(\mu_i T \sec\theta)} \qquad (12)$$

The variation of μ_i with wavelength for oxygen, carbon and hydrogen was taken from the work of Victoreen [8] to calculate $\mu_i(\theta)$.

The background scattering was measured for both the main scan and low angle scans in the absence of a sample and was less than 2% of the scattering over most of the angular range. The background was corrected for absorption by the sample before subtraction from the intensity data.

The scattered intensities include a component of multiply scattered photons, whereas the scattering theory is based on single scattering only. The problem of removing the multiply scattered component has been discussed by Wignall *et al* [9] who have shown that exact estimation of this component is impossible because of the prohibitive expense of computation. For this reason, corrections for this effect have often been neglected. However, numerical estimates of the fraction of double scattering, which is the major fraction of the multiple scattering, have been made [9] in the geometry of Fig. 1 using the methods of Warren and Mozzi [10]. It has been shown that in this geometry the fraction of double scattering $I_2(\theta)$ to single scattering, $I_1(\theta)$ increases with angle to a value ~ 0.1 at $\theta \sim 60°$. A first order correction may therefore be made as $I_2(\theta)$ is given to a good approximation [9] by

$$I_2(\theta) \simeq B \times I_1(\theta) \times \theta \qquad (13)$$

where B is a constant. Exact calculation of B is not possible, though first order calculations indicate that $B \sim 0.001$. A simulation of double scattering by the above methods for sample A is given in Fig. 3, showing that the linear approximation of Equation 13 gives a reasonable fit. A correction for double scattering based on Equation 13 is, therefore, made and the value

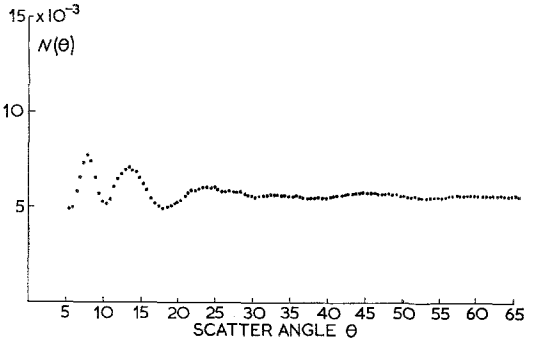

Figure 4 Normalization of the scattering data for sample A ($B = 0.0015$).

of B is chosen for best normalization behaviour. The value so chosen for sample A ($B \simeq 0.0015$) agrees within the experimental errors and the limits of the computational techniques with the value calculated for this sample ($B \simeq 0.002$).

The intensity of scattered radiation is given by [3]

$$cI_1(\theta) = NAT\left[\frac{\sum_{i=1}^{n} x_i f_i^2(\theta) + \sum_{i=1}^{n}\sum_{j=1}^{n} x_i x_j f_i(\theta) f_j(\theta) i_{ij}(\theta)}{a_c(\theta)} + \frac{\sum_{i=1}^{n} x_i I^i_{\mathrm{inc}}(\theta)}{a_i(\theta)}\right] \quad (14)$$

where the system consists of N atoms of n different species, with atomic concentrations x_i. $f_i(\theta)$ is the scattering factor, and $I^i_{\mathrm{inc}}(\theta)$ is the incoherent scattering of the i'th species, corrected by the Breit-Dirac recoil factor. $i_{ij}(\theta)$ is the partial interference function for species i and j and C/NAT is the normalization factor that converts the arbitrary units of the intensity measurements to electron units. As $\theta \to \infty$ $i_{ij}(\theta) \to 0$ and thus Equation 14 becomes

$$\frac{c}{NAT} = \lim_{\theta\to\infty} \frac{1}{I_1(\theta)}\left[\frac{\sum_{i=1}^{n} x_i f_i^2(\theta)}{a_c(\theta)} + \frac{\sum_{i=1}^{n} x_i I^i_{\mathrm{inc}}}{a_i(\theta)}\right]. \quad (15)$$

Assuming that the measured intensity $I_{\mathrm{sm}}(\theta)$ is made up of both single and double scattering, i.e.

$$I_{\mathrm{sm}}(\theta) \simeq I_1(\theta) + I_2(\theta) \quad (16)$$

and using Equations 13 and 16, then Equation 15 becomes

$$\frac{c}{NAT} = \lim_{\theta\to\infty}\left\{\frac{1 + B\theta}{I_{\mathrm{sm}}(\theta)}\left[\frac{\sum_{i=1}^{n} x_i f_i^2(\theta)}{a_c(\theta)} + \frac{\sum_{i=1}^{n} x_i I^i_{\mathrm{inc}}}{a_c(\theta)}\right]\right\} \quad (17)$$

Thus, if the normalization ratio, $N(\theta)$, is defined to be

$$N(\theta) = \frac{(1 + B\theta)}{I_{\mathrm{sm}}(\theta)}\left[\frac{\sum_{i=1}^{n} x_i f_i^2(\theta)}{a_c(\theta)} + \frac{\sum_{i=1}^{n} x_i I^i_{\mathrm{inc}}}{a_c(\theta)}\right]. \quad (18)$$

Then $N(\theta)$ should tend to a constant value c/NAT, as $\theta \to \infty$, with $B \simeq 0.001$. Fig. 4 shows the behaviour of $N(\theta)$ for sample A, using the dispersion corrected coherent scattering factors of Berghuis[11] and Stewart[12] and incoherent scattering factors of Keating and Vineyard [13], Sagel [14] and Freeman [15]. $N(\theta)$ exhibits the expected behaviour for all samples using values of $B \simeq 0.0015$, 0.0008 and 0.0008 for samples A, B and C respectively. These values are of the correct order of magnitude to account for the expected double scattering, and as expected were highest for sample A owing to its greater thickness.

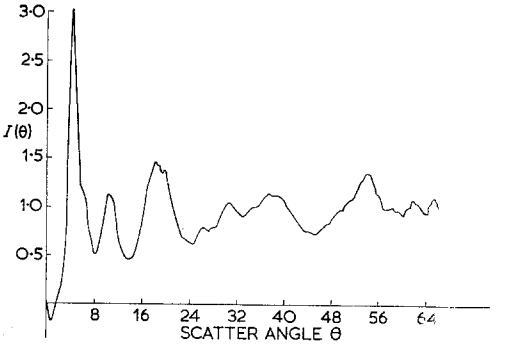

Figure 5 The interference function for sample A.

The average normalization constant $(C/NAT)_{\mathrm{av}}$ was chosen by averaging the values between $\theta = 30, 65°$ for each sample. The interference function $j(\theta)$ defined by Pings and Waser [3] is calculated from Equation 19. A typical plot (that for sample A) is shown in Fig. 5.

$$j(\theta) = j(s) = 1.0 + \frac{\left\{\left[I_{sm}(C/NAT)_{av}/(1 + B\theta)\right] - \left[\sum_{i=1}^{n} x_i I^i_{inc}/(a_i/\theta)\right] - \left[\sum_{i=1}^{n} x_i f_i^2(\theta)/(a_c(\theta)\right]\right\}}{\sum_{i=1}^{n} x_i f_i^2(\theta)} . \quad (19)$$

The corresponding RDF, $H(r)$ defined by Pings and Waser [3] is given by:

$$H(r) = \frac{1}{2\pi^2 \bar{\rho} r} \int_0^\infty s(i(s) - 1) \sin sr \, ds \quad (20)$$

and experimental RDF's were generated by means of an IBM Fourier transform routine. $\bar{\rho}$ is the mean atomic density for the system, i.e. the total number of atoms in the system divided by the volume occupied.

$H(r)$ as defined by Equation 20 required values of $sj(s)$ from 0 to infinity. However, in practice, data are available only over the range $s = \sim .15 \rightarrow \sim 16\text{Å}^{-1}$.

The truncation of $sj(s)$ at S_{max} will introduce spurious high frequency oscillations in the RDF and a standard procedure for eliminating these oscillations is to apply an exponential damping factor $e^{-\alpha^2 s^2}$, to $sj(s)$ before transformation. On physical grounds it is apparent that high frequency oscillations at low r (1Å $\leqslant r \leqslant$ 5Å) can represent real intra-molecular distances, and to avoid eliminating these peaks no damping factor is applied when considering this region. A careful comparison of the undamped data with the known molecular structure is necessary to check for the existence of truncation errors in this region. When considering the high r region of the RDF (15Å $\leqslant r \leqslant$ 80Å), however, we expect, on physical grounds, that high frequency oscillations cannot represent real physical features and the exponential damping factor may be used to eliminate the truncation errors.

Plots of the quantity $r\,H(r)$ versus r are shown in Figs. 6, 7 and 8 for samples A, B and C respectively and were obtained initially without damping $sj(s)$, i.e. with $\alpha = 0.0$.

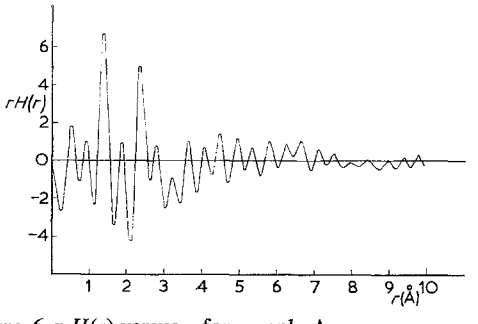

Figure 6 $r\,H(r)$ versus r for sample A.

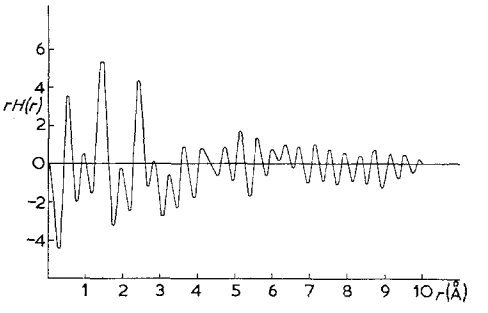

Figure 7 $r\,H(r)$ versus r for sample B.

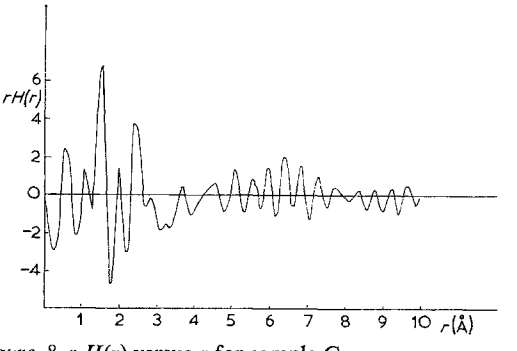

Figure 8 $r\,H(r)$ versus r for sample C.

Alternative methods of normalization [16] were used to calculate the normalization constant. The values obtained agreed to within 1% with those used to generate the RDFs of Figs. 6 to 8, whilst the RDFs generated via 20 agreed with those shown in Figs. 6 to 8 within the experimental error.

5. Discussion

In general the peaks observed in the RDF plot for a polymer should be attributable either to intramolecular atomic distances dependent upon the repeat unit, or to intermolecular atomic distances determined by the short range order or packing of the chains.

In the case of polycarbonate, crystallization

proceeds only very slowly over a restricted temperature range [17] so that both samples A and B are unlikely to show any appreciable degree of intermolecular order, i.e. no extensive packing of the polymer chains into highly ordered regions, so that inter-molecular spacings might be expected to remain ill defined. However, the intramolecular distances should be well defined at least for short distances, $1 \leqslant r \leqslant 6$Å.

The repeat unit of bisphenol-A polycarbonate is

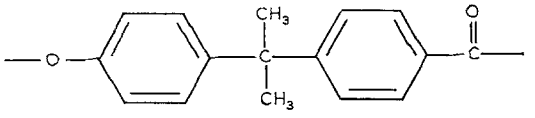

the assumed molecular conformation of this unit being given in Fig. 9 and was determined from the crystal structure of the polycarbonate [18]. It was considered that this unit would adopt the same conformation in the amorphous state for the following reasons. The bond angles about the centre carbon atom C (see Fig. 9) are fixed, and rotation of the benzene rings about the bonds C_1—C_2 and C_1—C_{11} is unlikely because of steric hindrance. Rotation of one repeat unit compared to the next may occur about the carboxyl group at bonds C_5—O_1, C_8—O_1 etc. allowing the polymer chain to adopt an overall random configuration whilst the inter-atomic spacings within the repeat unit remain largely unaffected. Thus, it should be possible to attribute some of the observed RDF peaks to intramolecular distances based on the conformation in Fig. 9. The inter-atomic distances calculated for the repeat unit are listed in Table I, together with the quantity

$$A_{ij} = \sum_{\text{uc}} \sum_{i} \frac{N_{ij}}{r_{ij}} Z_i Z_j \frac{\pi}{2}$$

where Z_i and Z_j are the atomic number of the i'th and j'th atom, r_{ij} is the distance between these atoms, n_{ij} is the number of neighbours in the j'th shell about the i'th atom and $\sum_{\text{uc}}$ refers to a summation over the unit of composition [5], in this case the repeat unit of the polymer.

This notation is taken from Mozzi and Warren [5] who show that A_{ij} is the area represented by the i—j bond in the RDF plot at r_{ij}. Comparison of Table I with Figs. 6 to 8 shows that all the observed peaks up to $r = 6.0$ together with their approximate relative intensities may be accounted for by intramolecular spacings, thus confirming that truncation of $sj(s)$ at S_{max} has contributed little spurious information to this region. The attribution of each inter-atomic distance to a specific peak is given in Table I.

The only feature not accounted for in this analysis is the peak falling at $r = 4.95$Å and $r = 5.17$Å for samples A and B respectively. This might be attributed to the inter-atomic distances resulting from the average intermolecular chain spacing of polycarbonate. Most high polymers comprised of C—C chains exhibit mean interchain distances of the order 4.5 to 6Å. For the particular case of polycarbonate the interchain spacing derived from the unit cell is 5.05Å [17]. It might be anticipated that an increase in the short range order in polycarbonate on partial crystallization would enhance this particular area of the RDF plot. It will be shown later, though, that inter-chain ordering manifests itself as a very broad hump in the RDF and that these features probably do not represent interchain ordering.

No attempt has been made to attribute specific high frequency peaks occurring at values of $r > 6$Å to specific inter-atomic distances mainly

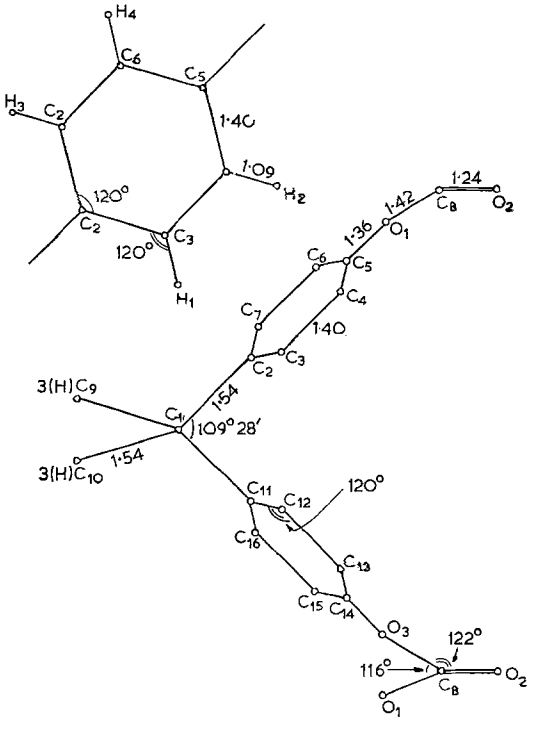

Figure 9 Assumed bond lengths and bond angles for the polycarbonate repeat unit.

for two reasons. Firstly the largely random arrangement of the polymeric chains means that the relative position of any part of neighbouring repeat units to each other is not known, so that only an average disordered configuration could be assumed. Secondly, and resulting from this, it is apparent that a large number of possible inter-atomic distances exist, such that all observed RDF peaks could have inter-atomic spacings attributed to them. However, it is not possible to determine the relative abundance of any specific inter-atomic spacing, or indeed to definitely confirm its presence, except by assuming all possible random configurations of the polymer chains within the steric limits of the structure. Thus attempts to identify peaks in the RDF plot at values of $r > 6$Å are not justified on the present samples.

Comparison of the experimental values of r for peaks attributed to the inter-atomic distances between hydrogen and other atoms with values calculated from published bond lengths, show that the experimental values are consistently lower than the calculated distances (see values in Table I). The above analysis has approximated the scattering system by using the independent scattering factors for each atom, though it is known that covalent bonding between atoms results in a concentration of the electron density along the bonds. The experiment effectively measures the bond length as the distance between effective centres of scattering power, i.e. electronic charge. This results in an apparent reduction in the "bond length" between hydrogen and other atoms, as the distortion of the electron orbital is more marked for hydrogen than for heavier atoms possessing more electrons, which in turn is reflected in the lower observed values of r for the RDF peaks associated with hydrogen inter-atomic distances.

In view of the satisfactory correlation of intramolecular inter-atomic distances to peaks at $r < 6$Å it is apparent that the RDF analysis is basically correct, and it is considered that significant short range intermolecular ordering should be readily resolved, if it was present in the samples.

Any intermolecular ordering is best seen by plotting $4\pi r^2\bar{\rho}H(r)$ over an extended range of r space and this is shown in Figs. 10, 11 and 12 for samples A, B and C respectively. As the ordinate is extremely sensitive to truncation errors at high r in view of the r^2 weighting, the ordinates are calculated with an appropriate damping

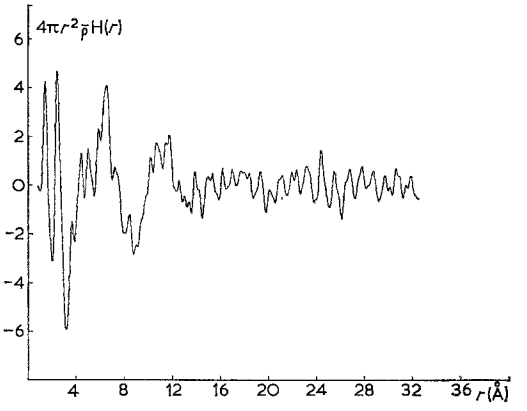

Figure 10 $4\pi r^2\bar{\rho}\ H(r)$ versus r for sample A.

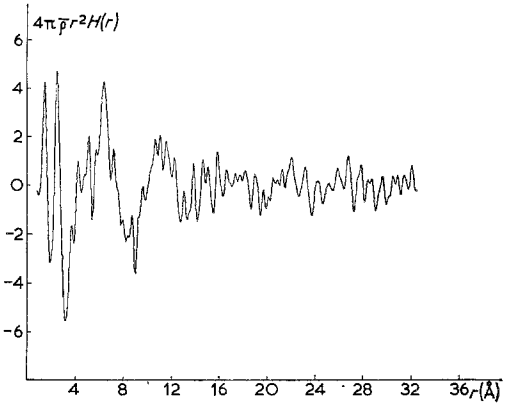

Figure 11 $4\pi r^2\bar{\rho}(Hr)$ versus r for sample B.

factor $\alpha = 0.112$. It is apparent from Figs. 10 to 11 that inter-chain ordering in samples A and B is present only vestigially as revealed by broad peaks at $r \simeq 5.5$Å and $r \simeq 11$Å upon which the intramolecular peaks are superimposed. These may be regarded as nearest neighbour chain interactions determined by the physical size of the polymer chains. It is apparent that there is no significant difference in the short range intermolecular order between samples A and B thus eliminating explanations of the change in impact properties which assume such re-ordering. This is consistent with the very small difference in density between samples A and B.

The striking difference between A and B on the one hand (Figs. 10 and 11) and C on the other (Fig. 12) lies in the very marked long range order in the RDF with a period $\sim$ 5.5Å. This feature undoubtedly represents intermolecular short range ordering in sample C. This apparently extends over distances of 50 to 60Å but the

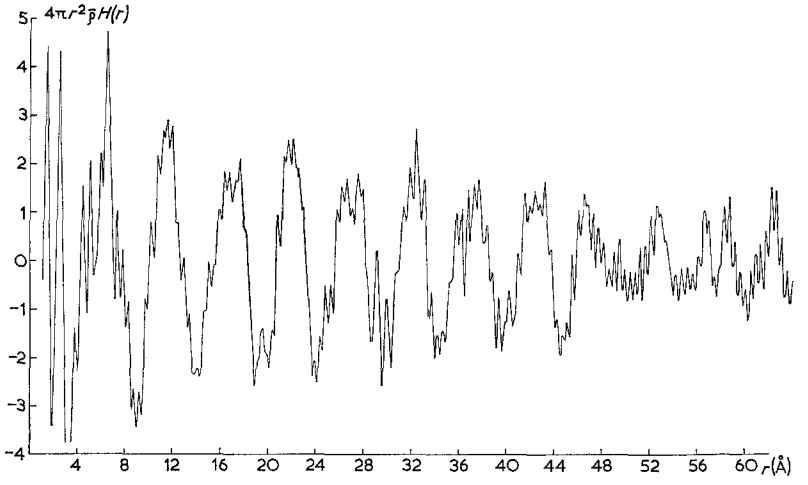

Figure 12 $4\pi r^2\bar{\rho}(Hr)$ versus r for sample C.

correlation is not observed at greater distances. This is not unexpected, as packing faults occur even in well ordered regions in highly crystalline polymers. Since the order in sample C represents quite a low "crystallinity" it is not surprising that intermolecular ordering is not detected at distances greater than ~ 60Å. However, the observed ordering is such that, it clearly demonstrates the sensitivity of the RDF technique to intermolecular ordering and reinforcing the conclusions concerning samples A and B.

Acknowledgements

Thanks are due to Dr J. A. J. Jarvis for helpful discussions concerning multiple scattering, to Dr D. C. W. Morley for supplying the samples and for helpful discussions, and to Mrs G. R. Woodward for valuable help with the data analysis system.

References

1. G. A. ALLEN, D. W. MORLEY, and T. WILLIAMS, *J. Mater. Sci.* **8** (1973) 1449.
2. J. WASER and V. SCHOMAKER, *Rev. Mod. Phys.* **25** (1953) 671.
3. C. J. PINGS and J. WASER, *J. Chem. Phys.* **48** (1968) 3016.
4. J. E. ENDERBY, D. M. NORTH, and P. A. EGELSTAFF, *Phil. Mag.* **14** (1966) 961.
5. R. L. MOZZI and B. E. WARREN, *J. Appl. Cryst.* **2** (1969) 164.
6. J. BOUKAL, *Eur. Polymer J.* **6** (1970) 17.
7. J. A. SOULES, W. I. GORDON, and C. H. SHAW, *Rev. Sci. Instrum.* **27** (1956) 12.
8. J. A. VICTOREEN, *J. Appl. Phys.* **20** (1949) 1141.
9. G. D. WIGNALL, W. E. MUNSIL, and C. J. PINGS, to be published.
10. B. E. WARREN and R. L. MOZZI, *Acta. Cryst.* **21** (1966) 459.
11. J. BERGHUIS, I. J. BERTHA, M. HAANAPPEL, M. POTTERS, B. O. LOOPSTRA, V. H. MACGILLAVRY, and A. L. VEENENDAAL, *ibid* **8** (1955) 478.
12. R. F. STEWART, E. R. DAVIDSON, and W. T. SIMPSON, *J. Chem. Phys.* **42** (1965) 3175.
13. D. T. KEATING and G. H. VINEYARD, *Acta. Cryst.* **9** (1956) 985.
14. K. SAGEL, "Tabellen zur Rontgenstrukturanalyse" (Springer-Verlag, Berlin, 1958).
15. A. J. FREEMAN, *Acta. Cryst.* **12** (1959) 261.
16. J. KROGH-MOE, *ibid* **1** (1958) 267.
17. A. SIEGMANN and P. H. GEIL, *J. Macromol. Sci-Phys.* **B4** (1970) 273.
18. A. PRIETZSCHK, *Kolloid Z.* **156** (1958) 8.

Received 13 March and accepted 25 April 1973.